

## Supporting Information

### Structure-Dependent Spin Polarization in Polymorphic CdS:Y

#### Semiconductor Nanocrystals

Pan Wang,<sup>a</sup> Bingxin Xiao,<sup>a</sup> Rui Zhao,<sup>a</sup> Yanzhang Ma<sup>b</sup> and Mingzhe Zhang<sup>\*a</sup>

<sup>a</sup> State Key Laboratory of Superhard Materials, Jilin University, Changchun 130012, China

<sup>b</sup> Department of Mechanical Engineering, Texas Tech University, Lubbock, Texas 79409, USA.

\* Corresponding Author. E-mail: zhangmz@jlu.edu.cn

#### 1. The process of gas-spray phase chemical reaction

We employed gas-spray phase chemical reaction to synthesize undoped and Y doped wurtzite CdS nanocrystals. All reagents were commercially available and used without further purification. In the first synthesis step of Y doped wurtzite CdS nanocrystals,  $Y(NO_3)_3$ ,  $Cd(COOCH_3)_2$ , PVP, and deionized water were mixed as a reactive solution. The molar ratio of  $Y^{3+}$  and  $Cd^{2+}$  was 0.12 in the reaction solution. For the first synthesis step of undoped wurtzite CdS nanocrystals,  $Cd(COOCH_3)_2$ , PVP, and deionized water were mixed as a reactive solution. The dosage of PVP is 0.1 mg per litre in the reaction solution. Then the pH of above well-mixed reaction solution was adjusted to the 7.0 using NaOH solution. In the second step, reaction solution was put into the ultrasonic nebulizer (Figure S1) to be atomized. Then the atomized reaction solution and excessive  $H_2S$  simultaneously entered into condenser tubes with circulating water (25 °C) by using gas pump and reacted with each other; the reaction products were collected in a flask placed in an ultrasonic bath to avoid agglomeration. Finally, reaction products were washed thrice with deionized water and anhydrous alcohol respectively by centrifugation, and dried in a nitrogen atmosphere.

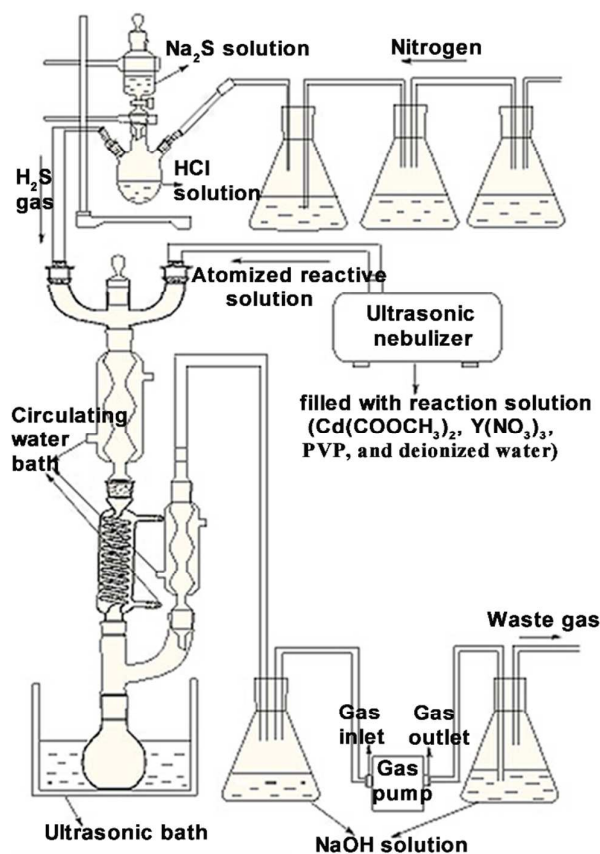


**Figure S1. Experimental setup of undoped and Y doped wurtzite CdS nanocrystals.**

Experimental setup of undoped and Y doped wurtzite CdS nanocrystals (wurtzite starting material) synthesized by gas-spray phase chemical reaction.

## **2. High pressure and high temperature experiment (HPHT) process**

High pressure and high temperature (HPHT) experiment process was depicted as follows: Y-doped wurtzite CdS nanocrystals synthesized by gas-spray phase chemical reaction were used as starting materials, and pressed into cylindrical samples with 2 mm in height and 3 mm in diameter. Then the samples were carried out on a cubic anvil apparatus (SPD-6×600T). The experiments were performed at 5.2 GPa and 100-300 °C (temperature interval was 100 °C) for a holding time of 30 min to gain 3 HPHT samples. The pressure was given by a calibration curve which was determined by phase transition pressures of bismuth, barium, and titanium. The temperature was measured by chromel-alumel type thermocouple.

## **3. Transmission electron microscopy (TEM) images of CdS polymorphs**

Figure S2 presents the transmission electron microscopy (TEM) image of the wurtzite starting material and the recovered rock-salt CdS polymorph. As shown in high-resolution TEM (HRTEM) image (Figure S2b) of the starting material, the measured interplanar spacings of 0.316 nm and 0.336 nm are consistent with (101) and (002) lattice planes of wurtzite CdS, respectively, in agreement with the selected-area electron diffraction (SAED) images (Figure S2a). The particle size of the wurtzite starting material is about 7-9 nm (Figure S2b). As the synthesis temperature is 300 °C and the pressure is 5.2 GPa, all the diffraction rings (Figure S2c) of the recovered sample are ascribed to the pure rock-salt CdS structure with no impurity phases. The measured interplanar spacing (Figure S2d) of 0.312 nm is a little less than 0.316 nm of (111) lattice planes of the rock-salt CdS structure, and the measured particle size is about 8-10 nm.

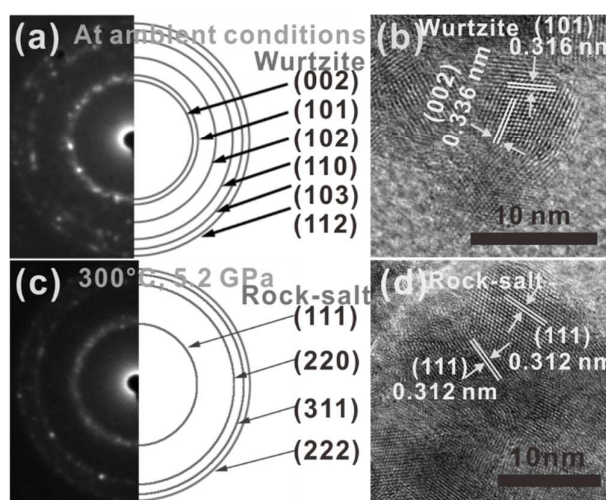


**Figure S2.** TEM images of CdS polymorphs. SAED patterns (a) and (c), HRTEM images (b) and (d), correspond to the wurtzite starting material, and the recovered rock-salt sample fabricated by the wurtzite starting material under 5.2 GPa and 300 °C, separately.

#### 4. X-ray photoelectron spectroscopy (XPS) analysis

The valence state of Y doped CdS nanocrystals synthesized by gas-spray phase chemical reaction has been further investigated by using XPS. In Cd 3d spectrum (Figure S3a), two peaks attributed to Cd 3d<sub>5/2</sub> and Cd 3d<sub>3/2</sub> at 405.2 and 411.9 eV indicate that Cd is in Cd<sup>2+</sup> state.<sup>1</sup> There is some overlap in Figure S2b due to the close binding energies of Y and S elements. The fitted two S 2p peaks

(Figure S3b) correspond to S  $2p_{3/2}$  and S  $2p_{1/2}$  at 161.5 and 162.9 eV, which suggests that the S is in  $S^{2-}$  state, in agreement with the reported value of CdS.<sup>2</sup> The fitted peak (Figure S3b) of Y  $3d_{5/2}$  at 158.5 eV manifests that Y is in  $Y^{3+}$  state,<sup>3</sup> excluding the possibility of Y metal clusters.

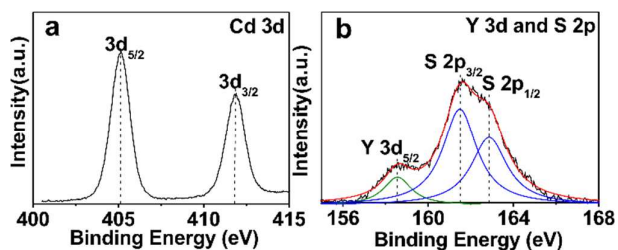


**Figure S3. XPS spectra of the Y doped CdS nanocrystals synthesized by gas-spray phase chemical reaction.** a) Binding energy of Cd 3d region; b) binding energies of Y 3d and S 2p regions respectively, each region contributed to by two peaks.

### 5. EDS analysis of CdS:Y polymorphs

As we can see from Figure S4-S5 and Table S1-S2 of energy-dispersive X-ray spectroscopy (EDS) analysis, Y contents are basically constant and about 0.2 atom% in wurtzite starting material and rock-salt CdS:Y nanocrystals. The sum of Y and Cd atomic concentrations are 49.59 and 47.21 which are less than the corresponding S atomic concentrations of 50.41 and 52.79 for wurtzite and rock-salt samples, respectively, indicating the existence of defects such as Cd vacancy, S antisite and S interstitial defects.<sup>4</sup> Moreover, the ratios between the above sum and S atomic concentrations for wurtzite and rock-salt CdS:Y samples are 0.98 and 0.89, separately, suggesting that the HPHT treatment is in favor of the formation of the above defects including vacancy defects, because the high pressure can compress the crystal lattice to rearrange the atoms and the high temperature can enhance the atomic thermal vibration.<sup>5,6</sup>

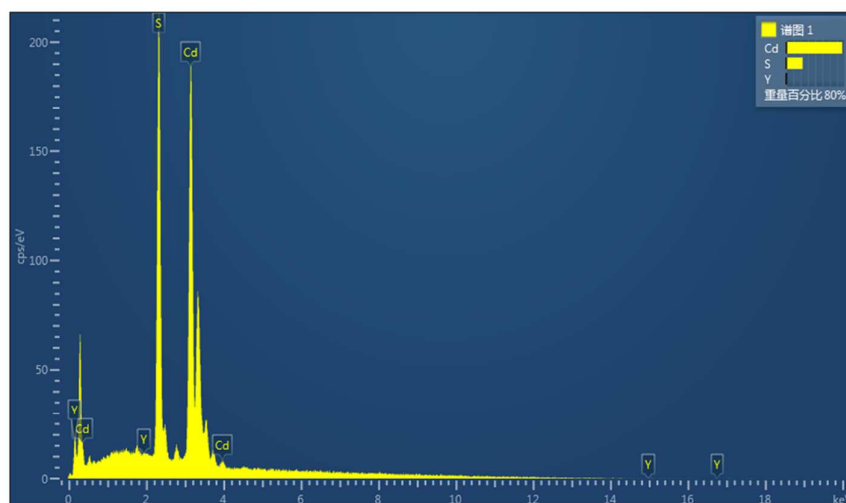


**Figure S4.** EDS spectrum of the wurtzite CdS:Y nanocrystals.

**Table S1.** Element content percentage of the wurtzite CdS:Y nanocrystals.

| Element | Weight (%) | Atom (%) |
|---------|------------|----------|
| S       | 22.49      | 50.41    |
| Y       | 0.22       | 0.18     |
| Cd      | 77.29      | 49.41    |
| Total   | 100.00     | 100.00   |

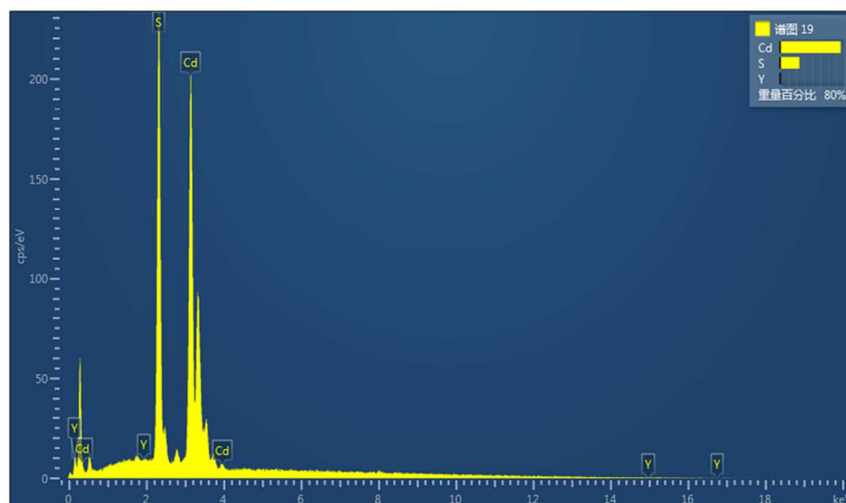


**Figure S5.** EDS spectrum of the rock-salt CdS:Y nanocrystals.

**Table S2.** Element content percentage of the rock-salt CdS:Y nanocrystals.

| Element | Weight (%) | Atom (%) |
|---------|------------|----------|
| S       | 24.20      | 52.79    |
| Y       | 0.25       | 0.20     |
| Cd      | 75.55      | 47.01    |

## 6. Model for analysis of magnetic origins of CdS:Y polymorphs

We select five model configurations for each structure to further explore the magnetic origins of CdS:Y polymorphs (Figure S6). Five configurations for each structure are: (a1, b1) a perfect supercell consisting of  $4 \times 4 \times 1$  wurtzite (lattice parameters,  $a = 4.111 \text{ \AA}$  and  $c = 6.726 \text{ \AA}$ ) or  $2 \times 2 \times 2$  rock-salt (lattice parameter  $a = 5.402 \text{ \AA}$ ) unit cells ( $\text{Cd}_{32}\text{S}_{32}$ ); (a2, b2) one Cd atom replaced with one Y dopant atom ( $\text{Cd}_{31}\text{YS}_{32}$ ); (a3, b3) one Cd vacancy created by removing one Cd atom ( $\text{Cd}_{31}\text{S}_{32}$ ); (a4, b4) one S atom in the Cd-substitutional position defect ( $\text{S}_{\text{Cd}}$ ) ( $\text{Cd}_{31}\text{S}_{33}$ ); (a5, b5) one S atom in the interstitial position defect ( $\text{S}_i$ ) ( $\text{Cd}_{32}\text{S}_{33}$ ). Then the spin-polarized density of states (DOS) and magnetic moments of above five configurations for two structures are calculated to analyze the origin of magnetism and the related magnetic mechanism, respectively. The Brillouin zones are sampled with a mesh of  $2 \times 2 \times 5$  for wurtzite system and  $3 \times 3 \times 3$  k-points for rock-salt system generated by the scheme of Monkhorst-Pack, respectively.

For wurtzite and rock-salt CdS systems, the chemical potentials  $\mu_{\text{Cd}}$  and  $\mu_{\text{S}}$  must satisfy the following growth condition. The defect formation energy is defined as:<sup>7</sup>

$$E^f = E_{\text{defect}}^{\text{tot}} - E_0^{\text{tot}} + n_- \mu_- - n_+ \mu_+ \quad (1)$$

Where  $E_{\text{defect}}^{\text{tot}}$  is the total energy of supercell containing the defect,  $E_0^{\text{tot}}$  is the total energy of host supercell,  $n_-$  is the number of Cd atoms substituted by defect and  $\mu_-$  is its chemical potential. Similarly,  $n_+$  is the number of defect atoms introduced into the supercell and  $\mu_+$  is the chemical potential.<sup>7</sup> For wurtzite and rock-salt CdS, the chemical potentials  $\mu_{\text{Cd}}$  and  $\mu_{\text{S}}$  must satisfy the following growth condition<sup>8</sup>

$$\mu_{\text{CdS}} = \mu_{\text{Cd}} + \mu_{\text{S}} \quad (2)$$

where  $\mu_{\text{CdS}}$  is the chemical potentials of wurtzite and rock-salt CdS systems.

Due to the excessive  $\text{H}_2\text{S}$  in experimental synthesis process, we consider the S-rich growth condition. At S-rich conditions, the chemical potential  $\mu_{\text{S}}$  is calculated from the solid  $\alpha\text{S}$ .<sup>8</sup> The chemical potential  $\mu_{\text{Cd}}$  is the obtained according to equation 2.

For one Cd vacancy defect in wurtzite and rock-salt  $\text{Cd}_{31}\text{S}_{32}$  system in comparison to ideal wurtzite and rock-salt  $\text{Cd}_{32}\text{S}_{32}$  system, respectively, the Cd vacancy defect energy is obtained according to equation 1 and 2,

$$E^f = E_{\text{Cd}_{31}\text{S}_{32}} - E_{\text{Cd}_{32}\text{S}_{32}} + \mu_{\text{Cd}} = E_{\text{Cd}_{31}\text{S}_{32}} - E_{\text{Cd}_{32}\text{S}_{32}} + \left(\frac{1}{32}E_{\text{Cd}_{32}\text{S}_{32}} - \mu_{\text{S}}\right). \quad (3)$$

For one Cd vacancy defect in wurtzite and rock-salt  $\text{Cd}_{30}\text{YS}_{32}$  system in comparison to wurtzite and rock-salt  $\text{Cd}_{31}\text{YS}_{32}$  system, respectively, the Cd vacancy defect energy is obtained according to equation 1 and 2,

$$E^f = E_{\text{Cd}_{30}\text{YS}_{32}} - E_{\text{Cd}_{31}\text{YS}_{32}} + \mu_{\text{Cd}} = E_{\text{Cd}_{30}\text{YS}_{32}} - E_{\text{Cd}_{31}\text{YS}_{32}} + \left(\frac{1}{32}E_{\text{Cd}_{32}\text{S}_{32}} - \mu_{\text{S}}\right). \quad (4)$$

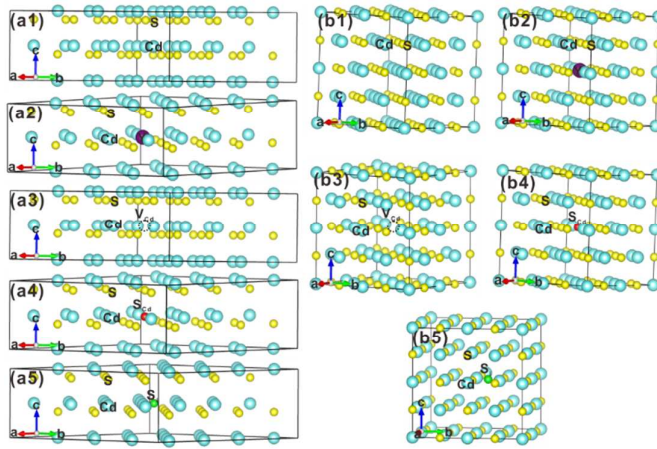


**Figure S6.** The five  $4 \times 4 \times 1$  wurtzite and  $2 \times 2 \times 2$  rock-salt CdS model configurations, for (a1, b1) the ideal system with no defect and dopant ( $\text{Cd}_{32}\text{S}_{32}$ ), (a2, b2) one Cd atom replaced with one Y dopant atom ( $\text{Y}_{\text{Cd}}$ ) ( $\text{Cd}_{31}\text{YS}_{32}$ ), (a3, b3) one Cd vacancy created by removing one Cd atom ( $\text{V}_{\text{Cd}}$ ) ( $\text{Cd}_{31}\text{S}_{32}$ ), (a4, b4) one S atom in the Cd-substitutional position defect ( $\text{S}_{\text{Cd}}$ ) ( $\text{Cd}_{31}\text{S}_{33}$ ), (a5, b5) one S atom in the interstitial position defect ( $\text{S}_{\text{i}}$ ) ( $\text{Cd}_{32}\text{S}_{33}$ ), separately.

## References

- (1) Fang, Y. M.; Song, J.; Zheng, R. J.; Zeng, Y. M.; Sun, J. J. Electrogenated Chemiluminescence Emissions from CdS Nanoparticles for Probing of Surface Oxidation. *J. Phys. Chem. C* **2011**, *115*, 9117-9121.
- (2) Guo, D. L.; Hua, H.; Yang, Q.; Li, X. Y.; Hu, C. G. Magnetism in Dopant-Free Hexagonal CdS Nanorods: Experiments and First-Principles Analysis. *J. Phys. Chem. C* **2014**, *118*, 11426-11431.
- (3) Gonzalo-Juan, I.; Escribano, J. A.; Castro, Y.; Sanchez-Herencia, A. J.; Fierro, J. L. G.; Ferrari, B. One-Pot Manufacture of Nanoparticle-Based Films in Aqueous Media via an Electric Field-Driven Assembly Process. *Green Chem.* **2014**, *16*, 3286-3296.

- (4) Gao, D. Q.; Yang, G. J.; Zhang, J.; Zhu, Z. H.; Si, M. S.; Xue, D. S.  $d^0$  Ferromagnetism in Undoped Sphalerite ZnS Nanoparticles. *Appl. Phys. Lett.* **2011**, *99*, 052502.
- (5) Baranov, P. G.; Soltamova, A. A.; Tolmachev, D. O.; Romanov, N. G.; Babunts, R. A.; Shakhov, F. M.; Kidalov, S. V.; Vul', A. Y.; Mamin, G. V.; Orlinskii, S. B.; Silkin, N. I. Enormously High Concentrations of Fluorescent Nitrogen-Vacancy Centers Fabricated by Sintering of Detonation Nanodiamonds. *Small* **2011**, *7*, 1533-1537.
- (6) Soltamova, A. A.; Il'in, I. V.; Shakhov, F. M.; Kidalov, S. V.; Vul', A. Y.; Yavkin, B. V.; Mamin, G. V.; Orlinskii, S. B.; Baranov, P. G. Electron Paramagnetic Resonance Detection of the Giant Concentration of Nitrogen Vacancy Defects in Sintered Detonation Nanodiamonds. *Jetp Lett.* **2010**, *92*, 102-106.
- (7) Wu, R. Q.; Peng, G. W.; Liu, L.; Feng, Y. P.; Huang, Z. G.; Wu, Q. Y. Ferromagnetism in Mg-Doped AlN from Ab Initio Study. *Appl. Phys. Lett.* **2006**, *89*, 142501.
- (8) Wu, J. C.; Zheng, J. W.; Wu, P.; Xu, R. Study of Native Defects and Transition-Metal (Mn, Fe, Co, and Ni) Doping in a Zinc-Blende CdS Photocatalyst by DFT and Hybrid DFT Calculations. *J. Phys. Chem. C* **2011**, *115*, 5675-5682.